12 Mar 1991, 10:30 am - 12:00 pm

G_{max} From Pressuremeter Tests: Theory; Chamber Tests; and Field Measurements

Peter M. Byrne
University of British Columbia, Vancouver, B.C., Canada

Francisco Salgado
University of British Columbia, Vancouver, B.C., Canada

J. A. Howie
University of British Columbia, Vancouver, B.C., Canada

Proceedings: Second International Conference on Recent Advances in Geotechnical Earthquake Engineering and Soil Dynamics, March 11-15, 1991, St. Louis, Missouri, Paper No. 1.25

G_{max} From Pressuremeter Tests: Theory; Chamber Tests; and Field Measurements

Peter M. Byrne, Francisco Salgado, and J.A. Howie
Department of Civil Engineering, University of British Columbia, Vancouver, B.C., Canada

SYNOPSIS: A method of analysis to predict the in situ maximum shear modulus $G_{max,o}$ from self-boring pressuremeter unload tests is presented. The method considers both the stress and void ratio changes induced by pressuremeter loading and the nonlinear stress-strain response upon unloading. The results are presented in the form of a chart that allows $G_{max,o}$ to be determined from the equivalent elastic unload modulus, G*, for a wide range of loading and unloading conditions. The analysis procedure is checked with chamber tests and field data and the results are found to be in good agreement provided factors to account for disturbance and anisotropy are considered.

INTRODUCTION

One of the soil parameters that can be derived from the Self-Boring Pressuremeter (SBP) is the equivalent elastic unload shear modulus, G*, which is obtained from the slope of the unload-reload pressuremeter loop as shown in Fig. 1. G*, however, is not equal to the maximum shear modulus, $G_{max,o}$ at the original stress state since it reflects both changes in the stress state due to expansion of the pressuremeter as well as high shear strains close to the face of the pressuremeter. $G_{max,o}$ is a fundamental soil parameter that is essential for dynamic analysis of soil structures. Previous researchers, Robertson (1982), Robertson and Hughes (1986) and Bellotti et al. (1989) have proposed methods for correcting the measured G* to obtain $G_{max,o}$ based upon an average stress and strain in the plastic zone. Herein, a more detailed analysis considering the complete variation in the stress and strain state is presented.

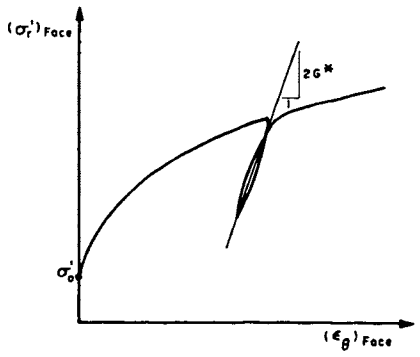

Fig. 1. Pressuremeter Unload Modulus, G*.

The proposed method involves the following steps: (i) An elastic- plastic analysis to determine the stress field caused by pressuremeter expansion. These stresses allow initial modulus values to be computed for unloading; (ii) A nonlinear elastic analysis to determine the displacement at the pressuremeter face upon unloading. These displacements are used to compute the equivalent elastic pressuremeter shear modulus, G*; and (iii) by comparing G* with $G_{max,o}$ for various levels of applied radial stress prior to unloading, and for various amounts of unload, a chart is generated from which $G^*/G_{max,o}$ can be obtained depending on the applied pressuremeter loading conditions.

The stress-strain relations used are an important factor in the analysis and hence these are described prior to presenting the analysis and results.

ASSUMED STRESS-STRAIN RELATIONS FOR SAND UPON UNLOADING

Upon unloading it is assumed that the initial shear modulus is the maximum shear modulus, G_{max}, and that the unloading curve is nonlinear and hyperbolic. Justification for these assumptions is presented in Figs. 2 and 3 from Byrne et al. (1987) based on triaxial tests by Negussey (1984). Figure 2 shows that Young's modulus upon unloading is nonlinear with strain, and Fig. 3 shows that the initial unload modulus is equal to the maximum modulus obtained from resonant column tests. Since E and G are related through Poisson's ratio, it is reasonable to assume the same behaviour for the shear modulus, G.

This indicates that the observed unload response of the pressuremeter could yield the in situ $G_{max,o}$ value if appropriate modifications for stress and strain levels are applied as discussed below.

G_{max} and Stress Level

Hardin (1978) proposed that G_{max} for sand can be expressed as follows:

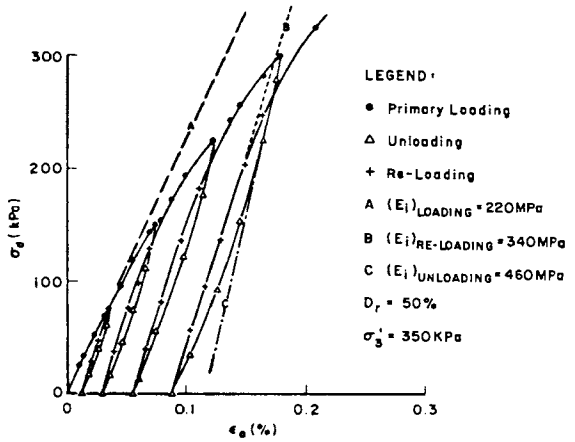

Fig. 2. Loading and Unloading Response in a Conventional Triaxial Path.

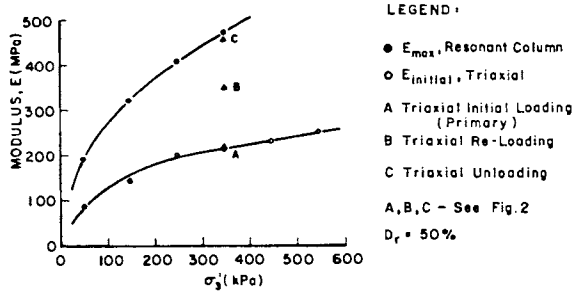

Fig. 3. A Comparison Between E_{max} and Various Initial Moduli E_i.

$$G_{max} = A \cdot F(e) \cdot p_a \left(\frac{\sigma_m'}{p_a}\right)^{0.5} \quad (1)$$

in which $\sigma_m' = 1/3\ (\sigma_1' + \sigma_2' + \sigma_3')$ termed the mean effective stress. The parameters A and F(e) depend on particle shape and void ratio, e, as follows:

$$\left.\begin{aligned} F(e) &= \frac{(2.17-e)^2}{1+e} \\ A &= 700 \end{aligned}\right\} \text{ Rounded sand} \quad (2)$$

and

$$\left.\begin{aligned} F(e) &= \frac{(2.97-e)^2}{1+e} \\ A &= 326 \end{aligned}\right\} \text{ Angular Sand} \quad (3)$$

and P_a = atmospheric presure in the units selected.

Hardin and Black (1966) and Hardin (1978) concluded that G_{max} was independent of deviator stress or stress ratio, depending only on σ_m'. However, more recent test data presented by Yu and Richart (1984) indicates that G_{max} depends on an average effective stress σ_{av}' that is somewhat different to σ_m'. In addition, it also depends on the stress ratio. Their proposed equation is:

$$G_{max} = A \cdot F(e) \cdot p_a \cdot \left(\frac{\sigma_{av}'}{p_a}\right)^{0.5} (1-0.3\ k_n^{1.5}) \quad (4)$$

in which $\sigma_{av}' = (\sigma_a' + \sigma_p')/2$, and σ_a' = the normal effective stress in direction of wave propagation σ_p' = the normal effective stress in direction of particle vibration. σ_{av}' may also be considered as the average effective stress in the plane in which the strains are induced.

The stress ratio effect is expressed in terms of k_n which is defined as follows:

$$k_n = (\sigma_1'/\sigma_3' - 1)/((\sigma_1'/\sigma_3')_{max} - 1) \quad (5)$$

where σ_1' and σ_3' are the major and minor principal effective stresses and correspond with σ_a' and σ_p'.

Equation 4 is in good agreement with the results of resonant column tests as shown in Fig. 4. It indicates that for a given sand

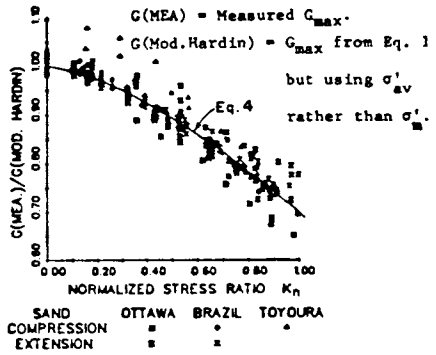

Fig. 4. Measured and Computed G_{max} Values.

at a given void ratio, G_{max} will increase with increased mean stress but will decrease with increased stress ratio. There will be a 30 percent reduction in G_{max} in zones where the stress ratio is a maximum, i.e. where the strength of the sand is fully mobilized. There may be a further change in G_{max} if the application of high stress ratios induces significant dilation or contraction of the sand that would affect the F(e) term in Eq. 4.

Upon unloading, the sand is assumed to respond in a nonlinear elastic manner as shown in Fig. 5. The unload stress-strain curve is assumed to be hyperbolic with the secant and tangent stiffness given by

$$G_s = G_{max}(1-SL) \quad (6)$$

$$G_t = G_{max}(1-SL)^2 \quad (7)$$

in which $SL = (\tau_L - \tau)/(\tau_L + \tau_f)$, where τ_L = the shear stress prior to unloading, τ = the current level of shear stress, τ_f = the shear

stress at failure. These stresses are shown in Fig. 5.

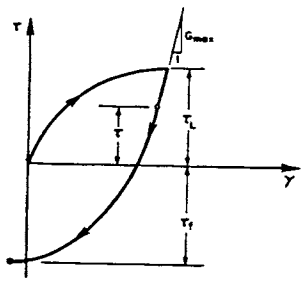

Fig. 5. Assumed Unload Stress-Strain Behaviour.

The secant modulus G_s as defined by Eq. 6 implies a modulus reduction with stress or strain level as shown in Fig. 6. The

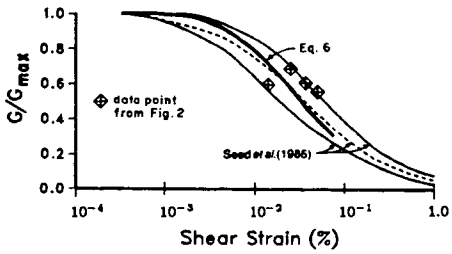

Fig. 6. G/G_{max} versus Shear Strain.

computed values of modulus reduction from the stress-strain loops of Fig. 2 are also shown on this figure and are in reasonable accord with Equation 6. Also shown in this figure are the average and upper and lower bounds from Seed et al. (1986). The equation chosen lies within the bounds specified by Seed et al.

ANALYSIS PROCEDURE

On expansion of the pressuremeter the stresses in the sand domain change as shown in Fig. 7. Initially, the radial stress, σ'_r

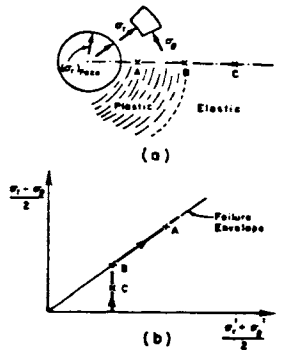

Fig. 7. Stress Strain After pressuremeter Loading.

increases while the circumferential stress, σ'_θ decreases. However, once the failure envelope is reached (point B) and a plastic zone develops, σ'_θ commences to increase in the plastic zone and the average effective stress $(\sigma'_r+\sigma'_\theta)/2$ increases as shown in the figure.

Since it is the unloading response of the pressuremeter that is of interest there would appear to be no need for an accurate stress and deformation analysis of the loading phase. However, based on the previous discussion, changes to the in situ state $G_{max,o}$ will occur due to changes in the average stress $\sigma'_{av} = 1/2\ (\sigma'_r+\sigma'_\theta)$, changes in the stress ratio, and perhaps changes in void ratio due to dilation or contraction. Hence it was necessary to carry out analyses to compute these changes.

The stresses prior to unloading were computed using a closed form solution. The deformations were assumed to occur under plane strain and follow an elastic-plastic stress-strain law. The analysis used has been described by Gibson and Anderson (1961), Ladanyi (1963), Vesic (1972) and Hughes et al. (1977), and herein only selected equations will be presented.

In the plastic zone the radial and circumferential effective stresses σ'_r and σ'_θ are linked by

$$\sigma'_r/\sigma'_\theta = \tan^2(45+\phi/2) = N \qquad (8)$$

The outer radius of the plastic zone R_p is given by

$$R_p = R_o\left[\frac{(\sigma'_r)_{face}}{\sigma'_o(1+\sin\phi)}\right]^{\left(\frac{1+\sin\phi}{2\sin\phi}\right)} \qquad (9)$$

in which R_o = the current pressuremeter radius, $(\sigma'_r)_{face}$ = the current effective radial stress at the pressuremeter face, and the σ'_o = the initial in situ horizontal stress. The stresses in the plastic zone, $(r < R_p)$, are given by:

$$\sigma'_r = \sigma'_{R_p} \cdot (R_p/r)^{1-N} \qquad (10)$$

$$\sigma'_\theta = \sigma'_r/N \qquad (11)$$

where the radial stress at the outer radius of the plastic zone σ'_{R_p} is given by

$$\sigma'_{R_p} = \sigma'_o(1+\sin\phi) \qquad (12)$$

Outside the plastic zone or within the elastic zone $(r > R_p)$, the stresses are given by

$$\sigma'_r = \sigma'_o(1 + R_p^2/r^2\ \sin\phi) \qquad (13)$$

$$\sigma'_\theta = \sigma'_o(1 - R_p^2/r^2\ \sin\phi) \qquad (14)$$

The above equations describe the stresses induced by expansion of the pressuremeter and these will be used in Equation 4 to compute G_{max} prior to unloading. In addition, there may be additional changes in G_{max} due to shear induced volume change and this will be addressed next.

Based upon Hughes et al., the shear strain distribution γ as a function of r in the plastic region is given by

$$\gamma = \left(\frac{R_p}{r}\right)^{n+1} \left(\frac{u_p}{R_p}\right)(1+n) \qquad (15)$$

where

$$u_p = R_p/2G\ \sigma_o\ \sin\phi \qquad (16)$$

$$n = (1 - \sin\nu)/(1 + \sin\nu)$$

and

ν = the dilation angle

Assuming that the dilation angle is constant with shear strain, the volumetric strain is given by

$$\epsilon_v = -\gamma \sin\nu \qquad (18)$$

and the change in void ratio by

$$\Delta e = (1 + e_o)\ \epsilon_v \qquad (19)$$

This change in void ratio was included in Equation 4 when computing the change in G_{max} prior to unloading.

Upon unloading the whole domain is assumed to behave in a nonlinear elastic manner. However, because the average stress $(\sigma'_r+\sigma'_\theta)/2$, the stress ratio σ'_r/σ'_θ, and the shear strain, γ, prior to unloading are different at every point within the domain, G_{max} will be different. In addition, the appropriate shear modulus will reduce with the level of unloading in accordance with Equations 6 or 7. Consequently, although the material is assumed to be elastic upon unloading, it is not homogeneous elastic and hence it is not appropriate to use closed form elastic equations to compute stress changes upon unloading. Herein a finite element analysis using a plane strain axisymmetric domain as shown in Fig. 8 was used.

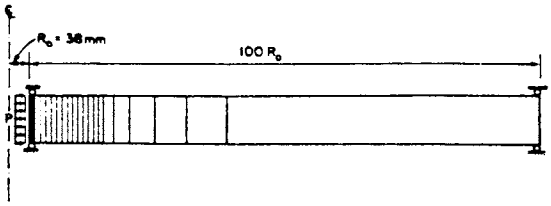

Fig. 8. Plane Strain Axisymmetric Finite Element Mesh.

The stresses σ'_r and σ'_θ in each element prior to unloading were computed for a given pressuremeter stress $(\sigma'_r)_{face}$ as described earlier. The shear induced changes in void ratio were computed from Eq. 19. From these stress and void ratio changes, G_{max} values were computed for each element based upon Eq. 4. The stress at the face of the pressuremeter was then unloaded in a series of small steps and a tangent stiffness corresponding to the average shear stress in the element was computed in accordance with Eq. 7.
The inward displacement at the face of the pressuremeter $(\Delta u)_{face}$ was computed for each step of unloading $(\Delta\sigma_r)_{face}$ and summed to allow the complete unloading response to be determined. The equivalent modulus G* was computed at various stages of unload and compared with $G_{max,o}$ computed from the initial stress and void ratio state, allowing the ratio $G^*/G_{max,o}$ to be determined for a range of $(\Delta\sigma_r)_{face}/(\sigma'_r)_{face}$ values. The process was then repeated using a range of $(\sigma'_r)_{face}$ values. This allowed the factor $\alpha_p = G^*/G_{max,o}$ to be computed as a function of both $(\sigma'_r)_{face}/\sigma'_o$ and $(\Delta\sigma_r)_{face}/(\sigma'_r)_{face}$ as shown in Fig. 9. The analyses were carried out over a range of σ'_o values as well as range of void ratio values ($.4<e<.7$) and the results were found to be insensitive to these variables. It was also found that shear induced void ratio effects on G_{max} were less than 5% for all loading conditions shown in Fig. 9. Dilation angles ranging between 0 for loose sands and 16° for dense sands were considered.

The proposed analysis presents a method of determining the in situ $G_{max,o}$ value from the secant modulus G* from the unload-reload pressuremeter loops which considers the variation in stress-strain and void state imposed by the pressuremeter. The results are expressed in terms of a single parameter α_p which is obtained from the chart of Fig. 9 and allows $G_{max,o}$ to be determined as follows:

$$G_{max,o} = G^*/\alpha_p \qquad (20)$$

The method is based upon analytical concepts and idealized soil behaviour and its validation requires comparison with measured data. Such data has recently become available.

Bellotti et al. (1989) presented both pressuremeter (ideal and self-bored) and resonant column and shear wave velocity tests for both laboratory and field conditions. Howie (1990) presented both full displacement pressuremeter and shear wave velocity tests for field conditions at McDonald's Farm in Richmond, B.C., Canada. The Bellotti and Howie data is used below for an evaluation of the proposed chart.

Bellotti et al. Data

G_{max} values were computed from the pressuremeter data using the chart of Fig. 9 and

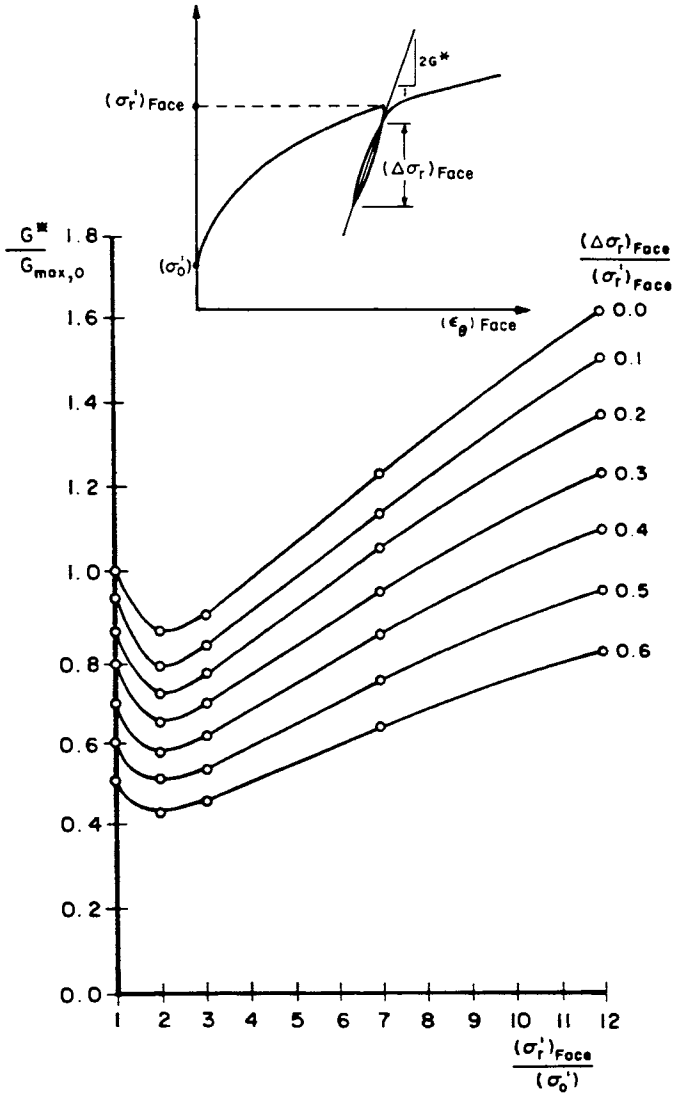

Fig. 9. Chart for Determination of $G_{max,o}$ from the Measrued G* Value.

Bellotti et al. Data

G_{max} values were computed from the pressuremeter data using the chart of Fig. 9 and compared with G_{max} from the resonant column (RC) or shear wave velocity tests. The comparison for the "ideal" pressuremeter chamber tests in which the pressuremeter was inserted prior to placing the sand is shown in Fig. 10 where it may be seen that G_{max} values from the resonant column tests are on average higher than those from the pressuremeter test by a factor of 1.25. This difference is largely due to the anisotropic nature of pluvially deposited sand. Pressuremeter tests involve strains in the horizontal plane whereas resonant column tests, G_{RC}, involve strain in the vertical plane. Bellotti et al. (1989) based on tests (Knox, 1982; Stokie and Ni, 1985; and Lee, 1986) indicate that the anisotropic factor $\alpha_A = G_{VH}/G_{HH} \approx 1.2$ in

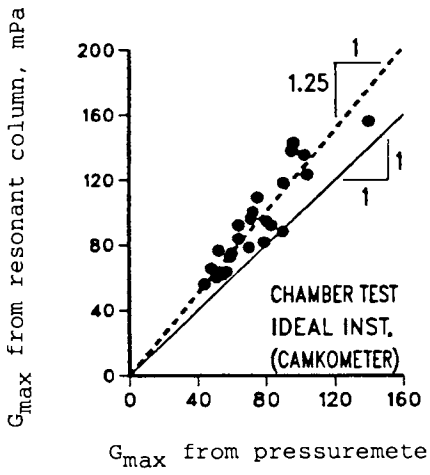

Fig. 10. Comparison of G_{max} Predicted and Measured. Chamber Test, Ideal Installation (Camkometer).

which G_{VH} = the maximum shear modulus in the vertical plane and G_{HH} = the maximum shear modulus in the horizontal plane. Thus the predicted G_{max} values from the pressuremeter are in good agreement with the expected G_{max} values for strains in the horizontal plane.

A similar comparison for "self-bored" pressuremeter chamber tests is shown in Fig. 11. It may be seen that the G_{max} values

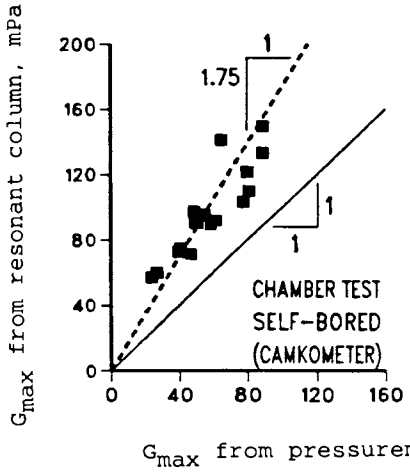

Fig. 11. Comparison of G_{max} Predicted an Measured. Chamber Test, Self-Bored (Camkometer).

from the resonant column test are on average 1.75 times higher than those from the pressuremeter test. This indicates that for this case the process of self-boring introduces a disturbance factor, $\alpha_D = 1.75/1.25 = 1.4$.

Comparisons of G_{max} values computed from self-boring pressuremeter and crosshole (CH) seismic tests for field conditions are shown in Figs. 12 and 13. It may be seen that the

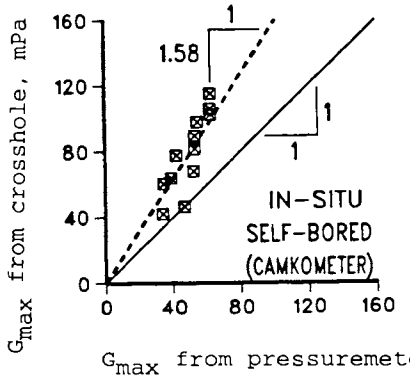

Fig. 12. Comparison of G_{max} Predicted and Measured. In-Situ, Self-Bored (Camkometer).

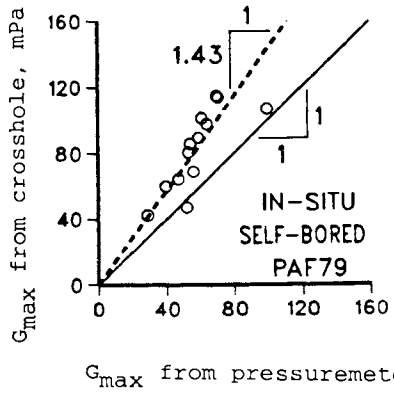

Fig. 13. Comparison of G_{max} Predicted an Measured. In-Situ, Self-Bored (PAF79).

G_{max} values from seismic exceed those computed from the pressuremeter by a factor of 1.58 for the Camkometer and 1.43 for the PAF-79 probe. If the disturbance factor α_D for the Camkometer is taken as 1.4, then the anisotropic factor, α_A = 1.58/1.4 = 1.13.

Belloti et al. (1989) suggest α_A = 1.2. Yan and Byrne (1989) based upon hydraulic gradient model tests and shear wave velocity measurements found α_A = 1.1, and the test data reported herein suggests α_A = 1.25 (Chamber tests, 'ideal' installation) and α_A = 1.13 (in situ tests, 'self-bored' installation). Based on the above four α_A values, an average value $(\alpha_A)_{av.}$ = 1.17 is obtained. This value is used below to interpret the data reported by Howie (1990).

Howie Data

G_{max} values were computed from the full displacement pressuremeter (FDPM) data reported by Howie using chart 9, and compared with G_{max} values obtained from downhole shear wave measurements. The predicted G_{max} values were found to be sensitive to $\sigma'_o = K_o\sigma'_v$. Detailed studies by Sully (1990) suggest K_o = 0.55 is appropriate for the sands at the McDonald Farm site and this value was used. The results are shown in Fig. 14, where it

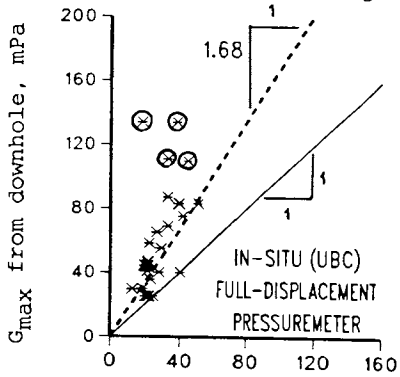

Fig. 14. Comparison of G_{max} Predicted and Measured. In-Situ, UBC Full-Displacement Pressuremeter.

may be seen that the G_{DH} values exceed those computed from the pressuremeter by a factor of 1.68. If the anisotropy factor α_A is taken as 1.17, then the disturbance factor for the FDPM is α_D = 1.68/1.17 = 1.43. The four circled data points shown in Fig. 14 lie well above the best fit line and were not considered in the above assessment because they correspond to tests carried out in a lightly cemented sand layer. They are included to indicate that the disturbance factor is likely significantly higher in cemented sands.

The data suggest that the disturbance factor, α_D, for the full-displacement and self-boring pressuremeters is approximately the same and equal to about 1.4. This is in agreement with both Robertson (1982) and Howie (1990) who found that the unload-reload modulus was approximately the same for full-displacement and self-boring pressuremeters.

Comparisons with laboratory and field data indicate that the proposed method can be used to predict the in situ $G_{max,o}$ value provided corrections are made for disturbance and anisotropy. The maximum shear modulus for horizontal loading G_{HH} can be obtained from pressuremeter tests as follows:

$$G_{HH} = \frac{G^*}{\alpha_p}\,\alpha_D \qquad (21)$$

in which G^* is the secant modulus from the pressuremeter unloading loop, α_p is the factor from the proposed chart (Figure 9) and α_D is the disturbance factor = 1.4 for both Camkometer and the full-displacement pressuremeter.

The maximum shear modulus for vertical loading, G_{VH} corresponds with shear moduli evaluated from seismic crosshole (CH) or downhole (DH) and can be expressed as follows:

$$G_{VH} = G_{CH} = G_{DH} = G_{HH}\alpha_A = \frac{G^*}{\alpha_P}\alpha_D\alpha_A \quad (22)$$

in which α_A is an anisotropic factor = 1.2.

SUMMARY

A procedure for analysing the unloading response of the pressuremeter has been presented. The analysis considers the effects of change in the average stress $(\sigma'_r+\sigma'_\theta)/2$, the stress ratio σ'_r/σ'_θ, and shear induced volume change on the maximum modulus. Results of the analyses are presented in a chart which allows the in situ, $G_{max,o}$ to be computed from the equivalent elastic shear modulus G* taking into account both the level of pressuremeter loading and unloading.

The predicted G_{max}, values from pressuremeter chamber and field tests (self-bored and full displacement) using the proposed chart are compared with G_{max} values obtained from resonant column and seismic tests and the results are found to be in good agreement provided factors are included to account for disturbance and anisotropic effects. The data suggest that the disturbance factor is about 1.4 for both the self-boring pressuremeter and the full-displacement pressuremeter. The anisotropic factor is about 1.2.

REFERENCES

BELLOTTI, R., GHIONNA, V., JAMIOLKOWSKI, M., ROBERTSON, P.K. and PETTERSON, R.W. Interpretation of moduli from self-boring pressuremeter tests in sand. Geotechnique, vol. 39, No. 2, 1989, 269-292.

BYRNE, P.M., CHEUNG, H. and YAN, L. Soil parameters for deformation analysis of sand masses. Cnd. Geot. J., vol. 24, No. 3, 1987, 366-376.

GIBSON, R.E. and ANDERSON, W.F. In situ measurements of soil properties with the pressuremeter", Civ. Eng. Pub. WKS Rev. 56, No. 658, May, 1961, 615-618.

HARDIN, B.O. and BLACK, W.L. Sand stiffness under various triaxial stresses. J. Soil Mech. and Found. Div., ASCE, vol. 92, No. SM2, 1966, 27-42.

HARDIN, B.O. The nature of stress-strain behaviour of soils. Proc., ASCE, Geo. Eng. Div. Specialty Conf. Earth. Eng. and Soil Dyn., Pasadena, Calif., vol. 1, 1978, 3-90.

HOWIE, J.A. Factors affecting the analysis and interpretation of full-displacement pressuremeter tests. Ph.D. Thesis, University of British Columbia, 1990.

HUGHES, J.M.O., WROTH, C.P. and WINDLE, D. Pressuremeter tests in sands. Geotechnique, vol. XXVII, No. 4, 1977, 455.

KNOX, D.P. Effect of state of stress on velocity of low amplitude shear wave propagating along principal stress direction in dry sand. Ph.D. Thesis, Texas University, 1982.

LADANYI, B. Evaluation of pressuremeter tests in granular soils. 2nd Pan American Conf., Soil Mech. Found. Eng. 1, 1963, 3-20.

LEE, S.H.H. Investigation on low amplitude shear wave velocity in anisotropic material. Ph.D. Thesis, Texas University, 1986.

NEGUSSEY, D. An experimental study of the small strain response of sand. Ph.D. Thesis, University of British Columbia, Vancouver, B.C., Canada, 1984.

ROBERTSON, P.K. In situ testing of soil with emphasis on its application to liquefaction assessment. Ph.D. Thesis, University of British Columbia, 1982.

ROBERTSON, P.K. and HUGHES, J.M.O. Determination of properties of sand from self-boring pressuremeter test. Proc. 2nd Int. Symp. on the Pressuremeter and its Marine Applications, Austin, Texas. American Society for Testing and Materials, 1986, 283-302.

STOKOE, K.H. and NI, F.H. Effects of stress state and strain amplitude on shear modulus of dry sand. Proc. 2nd Symp. Interaction of Non-nuclear Munitions with Structures, Panama City Beach, 1985, 407-412.

SULLY, J. Private communication, September 1990.

VESIC, A.S. Expansion of cavities in infinite soil mass. J. Soil Mech. and Found. Div., ASCE, vol. 98, No. SM3, 1972, 265-290.

YAN, L. and BYRNE, P.M. Simulation of downhole and crosshole seismic tests on sand using the hydraulic gradient similitude method. Soil Mech. Series No. 132, Dept. of Civil Engineering, University of British Columbia, Vancouver, Canada, Oct. 1989.

YU, P. and RICHART, F.E. Stress ratio effects on shear modulus of dry sands. J. Geot. Eng., vol. 110, No. 3, March 1984, 331-345.